# Highly efficient tunable terahertz all-dielectric metasurface absorber based on high mode

Song Gao,[1] Jianchun Xu,[1] Jinqing Cao,[1] Huiming Yao,[1] S. Eltahir Ali,[2] Hala M. Abo-Dief,[2] Abdullah K. Alanazi,[3] Chuwen Lan,[1,*] Hassan Algadi,[5,6] Xiaojun Zhai,[4,*]

[1] State Key Laboratory of Information Photonics and Optical Communications, School of Science & School of Information and Communication Engineering,Beijing University of Posts and Telecommunications,Beijing,100876,China

[2] Department of Science and Technology, University College-Ranyah, Taif University, P.O. Box 11099, Taif 21944, Saudi Arabia

[3] Department of Chemistry, College of Science, Taif University, P.O. Box 11099, Taif 21944, Saudi Arabia

[4] School of Computer Science and Electronic Engineering, University of Essex, Colchester CO4 3SQ, UK

[5] College of Materials Science and Engineering, Taiyuan University of Science and Technology, Taiyuan, 030024, China

[6] Department of Electrical Engineering, Faculty of Engineering, Najran University, Najran, 11001, Saudi Arabia

[*]Correspondence to lanchuwen@bupt.edu.cn; xzhai@essex.ac.uk

**Keywords**: Terahertz, All-dielectric metasurface, Tunable, Liquid crystal

## Abstract

All-dielectric terahertz metasurface absorbers have aroused widespread attention over the past few years for their flexible design concepts and excellent absorbing properties. However, the existing all-dielectric terahertz metasurface absorbers are subjected to poor tunability. In this study, a high-efficiency magnetically tunable terahertz all-dielectric metasurface absorber scheme is proposed based on high modes. In this paper, the all-dielectric metasurface is compounded with the liquid crystal, and the device can be tunable by different applied magnetic fields. The results show that the absorption peak of the device is very sensitive to different applied magnetic fields. By studying the tunable performance of the first three levels of Mie resonance peaks of the absorber, we found that the device has efficient tunability in high mode and optimized the design of the all-dielectric metasurface absorber with the tuning figure of merit (FOM) of up to 6.67. This scheme shows the advantages of simple fabrication, low cost,

and high integration, and it will provide a novel idea for the design of highly efficient terahertz tunable all-dielectric metasurface absorbers.

## 1 Introduction

Terahertz wave refers to an electromagnetic wave between microwave and far-infrared bands, and its spectrum ranges from 0.1 to 10 THz. Electromagnetic waves in the infrared and microwave bands have been extensively recognized and applied [1-5], whereas there are relatively few explorations and studies in the terahertz band. Since terahertz technology has only begun to receive attention over the past few years, related materials, devices, and systems are not yet mature. Over the past few years, the emergence of metamaterials (metasurfaces) has played a major role in promoting the research field of electromagnetic materials [6-9]. Metamaterials are artificially structured materials composed of aligned subwavelength structures that can be artificially designed to obtain unusual electromagnetic properties in the terahertz frequency range [10]. Unlike traditional materials, their electromagnetic properties depend largely on the geometric parameters and arrangement of the unit cells, rather than the material itself. Given the above property, researchers can tune their electromagnetic properties in the sub-wavelength dimension. In the past ten years, although great progress has been made in subwavelength metallic metamaterials [11], there are still some disadvantages, such as severe ohmic loss and anisotropic properties [12-14]. Over the past few years, all-dielectric metamaterials based on Mie resonances [15], which consist of periodic or aperiodic dielectric resonators made of high-index and low-loss dielectric materials, have become increasingly popular. It has aroused considerable attention for its low intrinsic loss, simple structure, and good compatibility with micromachining [16-18].

As to the terahertz all-dielectric metamaterials, some progress has been made and various devices have been developed [19-22]. Researchers use all-dielectric metamaterials to realize isotropic perfect wave absorbers, and discover their application potential in imaging [23], polarization detection [24], and so forth. This type of structure is generally limited by the

bandwidth, and the electromagnetic response of the metamaterial after the structure is determined will be determined as well, and its poor tunability and other reasons significantly limit its application. Therefore, according to the design structure of different materials [25-30], several solutions have been proposed (e.g., ferroelectric materials [31], ferromagnetic materials [32]). However, these tunable materials have different limitations, some are difficult to achieve a balance between the performance of the material itself and tunability, some are high preparation cost, poor integration, and some are tunable performance is limited by temperature, external force and other conditions.

To solve these problems, in this article, we propose a high mode tunable all-dielectric metasurface based on liquid crystal properties. The metasurface is compounded with the liquid crystal, and using the property of liquid crystal anisotropy, magnetic fields are applied in three directions perpendicular to each other in the all-dielectric metasurface. When the magnetic field strength is significantly greater than the threshold for repositioning the liquid crystal molecules to rearrange, the liquid crystal molecules will be arranged along the direction of the magnetic field [33], thus changing the dielectric properties of the metasurface and realizing the dynamic tunability of the absorption peak of the all-dielectric metasurface.

## 2 Structural design and simulation

Mie scattering refers to a type of elastic scattering. The energy between particles is transferred to each other during scattering. The above theory analyzes the scattering phenomenon of spherical particles in a homogeneous medium under the irradiation of a monochromatic plane wave by matching Maxwell's equations and boundary conditions to yield an accurate solution. Thus, the all-dielectric metasurface has two modes of resonance: electrical and magnetic. The Mie resonance of all-dielectric materials serves as a mechanism to generate electromagnetic resonance based on displacement current, thus laying a theoretical basis for all-dielectric metasurfaces in the terahertz range. The size design of all-dielectric resonators can be similar to the terahertz wavelength and the scattering intensity will vary with the size of the particle.

With the increase of the size of the particle, the scattering intensity is increased, whereas the shape of the particle should be strictly designed to be spherical. The Mie scattering theory suggests that the scattering field of the incident electromagnetic wave passing through the medium particles can be decomposed into a multi-dipole combination mode, and the m-th order electric/magnetic scattering coefficients are expressed as $a_m$ and $b_m$ [34]:

$$a_m = \frac{n\psi_m(nx)\psi_m^{'}(x) - \psi_m(x)\psi_m^{'}(nx)}{n\psi_m(nx)\xi_m^{'}(x) - \xi_m(x)\psi_m^{'}(nx)} \tag{1}$$

$$b_m = \frac{n\psi_m(nx)\psi_m^{'}(x) - \psi_m(x)\psi_m^{'}(nx)}{n\psi_m(nx)\xi_m^{'}(x) - n\xi_m(x)\psi_m^{'}(nx)} \tag{2}$$

where $r_0$ denotes the radius of the medium sphere; $n$ represents the refractive index of the medium sphere, $x = k_0 r_0$ ; $k_0 = \frac{\omega}{c} = \frac{2\pi}{\lambda}$ expresses the wave vector in vacuum. $\psi_m$ and $\xi_m$ represent Riccati-Bessel functions.

Lewin studied the electromagnetic response behavior, effective permittivity and effective permeability of composite materials formed by non-loss dielectric and magnetic particle spheres dispersed in another continuum using effective medium theory and electromagnetic scattering theory, which are expressed as follows [35]:

$$\varepsilon_{eff} = \varepsilon_h \left[ 1 + \frac{3v}{\frac{F(\theta) + 2K_e}{F(\theta) - K_e} - v} \right] \tag{3}$$

$$\mu_{eff} = \mu_h \left[ 1 + \frac{3v}{\frac{F(\theta) + 2K_m}{F(\theta) - K_m} - v} \right] \tag{4}$$

$$K_e = \frac{\varepsilon_h}{\varepsilon_p} \tag{5}$$

$$K_m = \frac{\mu_h}{\mu_p} \tag{6}$$

$$v = \frac{4}{3}\pi\left(\frac{r_0}{l}\right)^3 \tag{7}$$

$$F(\theta) = \frac{2(\sin\theta - \theta\cos\theta)}{(\theta^2 - 1)\sin\theta + \theta\cos\theta} \tag{8}$$

$$\theta = k_0 r_0 \sqrt{\varepsilon_p \mu_p} \tag{9}$$

Where $\varepsilon_p$ and $\mu_p$ denote the relative permittivity and permeability of the microspheres, respectively; $\varepsilon_h$ and $\mu_h$ represent the relative permittivity and permeability of the continuum, respectively; $l$ expresses the lattice constant. The theory highlights that in the magnetic resonance mode, the electromagnetic wave induces a circular displacement current in the medium microsphere; the microsphere is equivalent to a magnetic dipole while generating a magnetic response; the equivalent magnetic dipole and the electromagnetic field exert a resonance effect, thus making the medium Microspheres are atom-structured metasurfaces with possibly negative values of $\mu_{eff}$ . Furthermore, in the electric resonance mode, the metasurface achieves a $\varepsilon_{eff}$ that can be negative.

After the constituent materials are determined, since the electromagnetic properties of the metasurface are primarily dependent on the design of the structure, the electromagnetic properties of the metasurface will be determined once the structure is determined, and its adjustability is poor. Based on this problem, in this study, the liquid crystal solution is combined with the all-dielectric metasurface, and the electromagnetic properties of the liquid crystal are dynamically adjusted by an external static magnetic field to achieve dynamic tuning of the resonant peak of the all-dielectric metasurface absorber.Through theoretical calculation and empirical analysis, we propose a tunable terahertz all-dielectric metasurface absorber, the unit cell structure of which is shown in Fig. 1(a). The structure consists of a polyimide/ceramic dielectric microsphere array with a thin gold film on the polyimide bottom. The top of the device is a polyimide film, and the middle part is filled with liquid crystal molecules. The geometric

parameters of the structure are: lattice constant $P_x = P_y = 120$ μm, and the thickness of the gold film is set as 5 μm. The thickness of the polyimide (PI) tape is set as 5 μm, and the dielectric

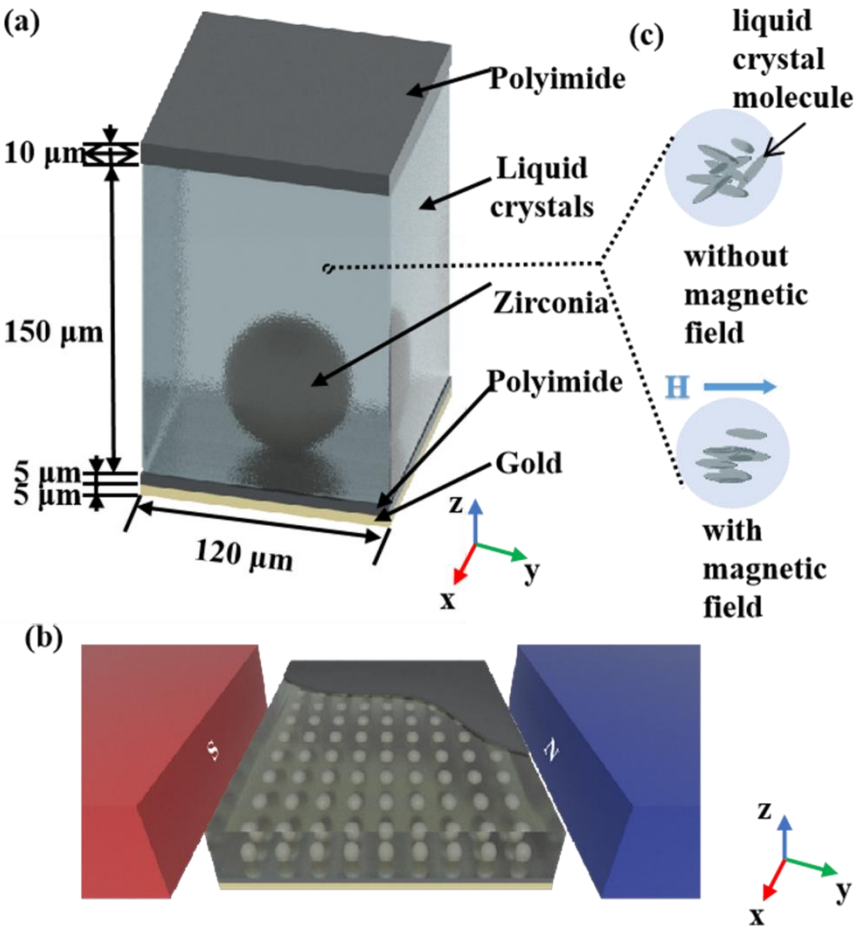


**Fig. 1** (a) Schematic diagram of the unit cell structure of the all-dielectric metasurface. To be specific, the lattice constant is 120 μm, the bottom yellow part is a gold film with a thickness of 5 μm, and the gray part. refers to a layer of polyimide (PI) tape with a thickness of 5 μm, and the middle blue part above the PI tape is liquid crystal. The thickness reaches 150 μm. The red part wrapped by the liquid crystal is zirconia spherical particles with a radius of 30 μm. The gray part on the top refers to a layer of polyimide (PI) tape with a thickness of 5 μm and just sticks to the liquid crystal to fix the liquid crystal. (b) Schematic diagram of all-dielectric metasurface model based on liquid crystal under external magnetic field. (c) The orientation of liquid crystal molecules with and without magnetic field

constant is set as 3 + 0.01i. The radius of the zirconia set as 5 μm, and the dielectric constant is set as 3 + 0.01i. The radius of the zirconia microspheres is set as 30 μm, and the dielectric constant is set as 32 + 0.05i. The thickness of the liquid crystal is set as 150 μm, and the dielectric constant in the respective direction is 2.6896 under no magnetic field. When an external magnetic field is applied, the dielectric constant of the liquid crystal is 3.0276 in the direction of the magnetic field, and 2.5281 in the other two directions. The thickness of the polyimide (PI) tape on the gray part of the uppermost layer is set as 10 μm, and the dielectric constant is set as 3 + 0.01i. The boundary condition is that the *x* direction is the direction of the electric field, and the *y* direction is the direction of the magnetic field.

The all-dielectric metasurface is immersed in liquid crystals. The liquid crystal molecules are parallel to the direction of the magnetic field when the external magnetic field is large enough to exceed the threshold required to reorient the liquid crystal nematic molecules, as presented in Fig. 1(c). The dielectric constant tensor ($\varepsilon_x$, $\varepsilon_y$, $\varepsilon_z$) is adopted to express the electromagnetic properties of liquid crystals. To be specific, the dielectric constants perpendicular to and parallel to the directions of liquid crystal molecules are expressed as $\varepsilon_\perp$ and $\varepsilon_{//}$, respectively. When no external magnetic field is applied, liquid crystal is an isotropic medium, and its dielectric constant tensor is expressed as ($\varepsilon_i$, $\varepsilon_i$, $\varepsilon_i$). It is assumed that liquid crystal molecules can be positioned by a uniform magnetic field. When the magnetic field is set along the x direction, the permittivity tensor is expressed as ($\varepsilon_{//}$, $\varepsilon_\perp$, $\varepsilon_\perp$). After repositioning, the liquid crystal has an ordinary refractive index of 1.59 ($n_o$) and an extraordinary refractive index of 1.74 ($n_e$). When the liquid crystal becomes isotropic, the refractive index is expressed as $n_i = (2n_o + n_e)/3 = 1.64$. When there is no external magnetic field, the liquid crystal permittivity tensor is expressed as ($\varepsilon_i$, $\varepsilon_i$, $\varepsilon_i$), where $\varepsilon_i = n_i^2$. Accordingly, the electromagnetic properties of the liquid crystal can be adjusted by changing the direction or

strength of the external magnetic field, such that the electromagnetic properties of the all-dielectric metasurface completely immersed in the liquid crystal are regulated. Furthermore, the Mie resonance induced in the metasurface can be adjusted by the external magnetic field, and its tunability is significantly susceptible to external magnetic field control.

**Table 1** Initial values of all-dielectric metasurface structural parameters

| Lattice constant (μm) | Microsphere radius (μm) | Spherical dielectric constant | Liquid crystal thickness (μm) | PI tape thickness (μm) | PI tape dielectric constant | Upper PI tape thickness (μm) | Upper PI tape dielectric constant |
|---|---|---|---|---|---|---|---|
| 120 | 30 | 32 | 150 | 5 | 3 | 10 | 3 |

The respective structural parameter is taken as a variable, and its initial value is listed in Table 1. The four external field environments are respectively no external magnetic field, external magnetic field along *x* direction, external magnetic field along *y* direction and external magnetic field along *z* direction.

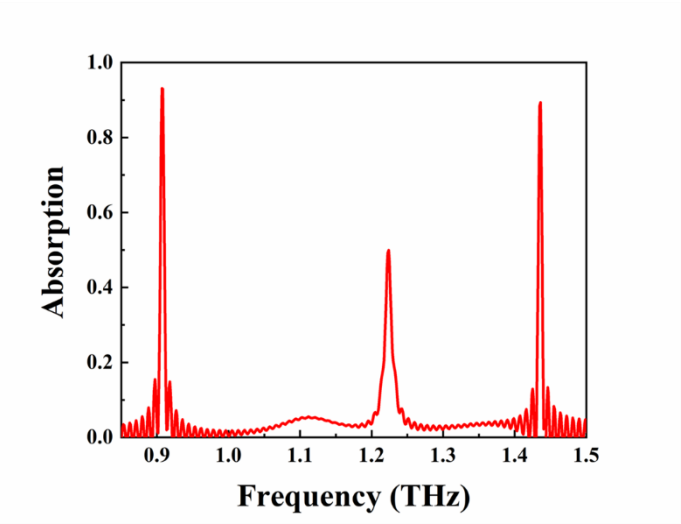


**Fig. 2** In the absence of any external field, the absorption caused by the first three Mie resonances of the initially designed metasurface absorber is simulated, and the simulated frequency range is 0.85-1.50 THz

The model is built according to the initial parameters of the absorber. To further study the tunable performance of the all-dielectric absorber, the absorption caused by the first three Mie resonances will be simulated, as presented in Fig. 2. At this time, the absorption peak 0.931 caused by the first Mie resonance appears at 0.907 THz; the absorption peak 0.499 caused by the second Mie resonance appears at 1.223 THz; the absorption peak 0.894 caused by the third Mie resonance appears at 1.433 THz.

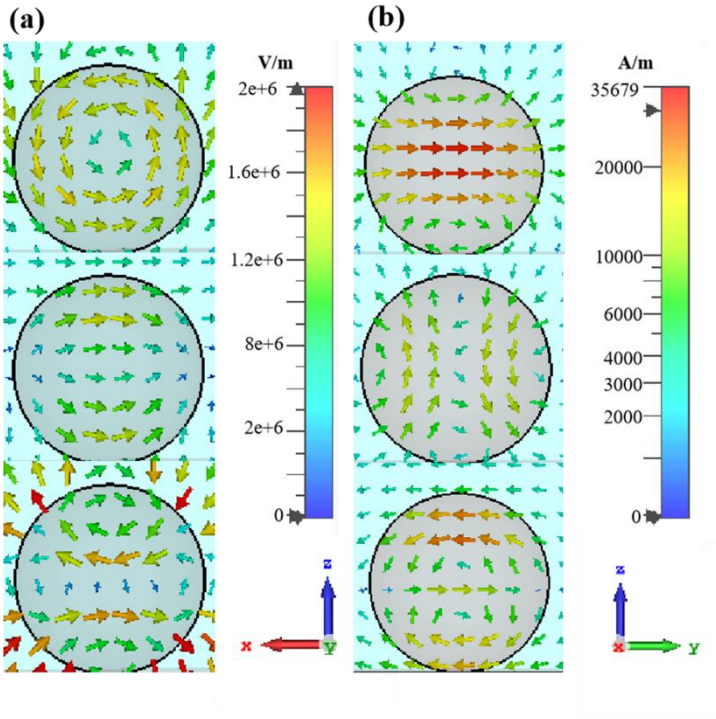


**Fig. 3** (a) From top to bottom are the electric field distributions of the first three Mie resonance peaks, where the viewing angle is selected from the bottom and along the *y*-axis (magnetic field direction). (b) From top to bottom are the magnetic field distributions of the first three Mie resonance peaks, where the left side of the viewing angle is selected along the *x*-axis (electric field direction)

As depicted in Fig. 3, in the electric field distribution of the first-order Mie resonance, the rotating electric field in the microsphere oscillates along the *y*-axis (magnetic field direction), and the magnetic field distribution of the first-order Mie resonance can display a significant linear magnetic field distribution. Moreover, the all-dielectric metasurface resonator at this frequency induces the first-order Mie resonance as magnetic resonance. In the magnetic field

distribution of the second-order Mie resonance, the rotating electric field in the left and right hemispheres of the microsphere simultaneously oscillates along the *x*-axis (electric field direction), and the electric field distribution of the second-order Mie resonance displays a significant linear distribution. At this frequency, the all-dielectric metasurface resonator induces the second-order Mie resonance as electric resonance [36]. In the electric field distribution of the third-order Mie resonance, the electric field rotating in the upper and lower hemispheres of the microsphere oscillates along the *y*-axis (magnetic field direction) simultaneously, and the electric field rotating in the middle part of the microsphere oscillates in the opposite direction. In the third-order Mie resonance, the resonant magnetic field distribution can be considered an overall linear magnetic field distribution. At this frequency, the all-dielectric metasurface resonator induces the third-order Mie resonance as a magnetic resonance. According to the Mie resonance theory, the electromagnetic resonance inside the all-dielectric resonator causes the absorption of electromagnetic waves by the metasurface. This is the basis for studying the work of the all-dielectric absorber, which is verified by the analysis of Fig. 3.

## 3 Simulation results and analysis

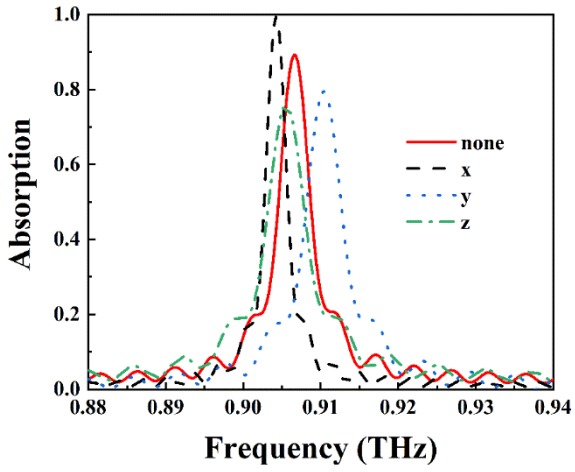


**Fig. 4** Absorptivity caused by the first-order Mie resonance of the absorber under four external field environments

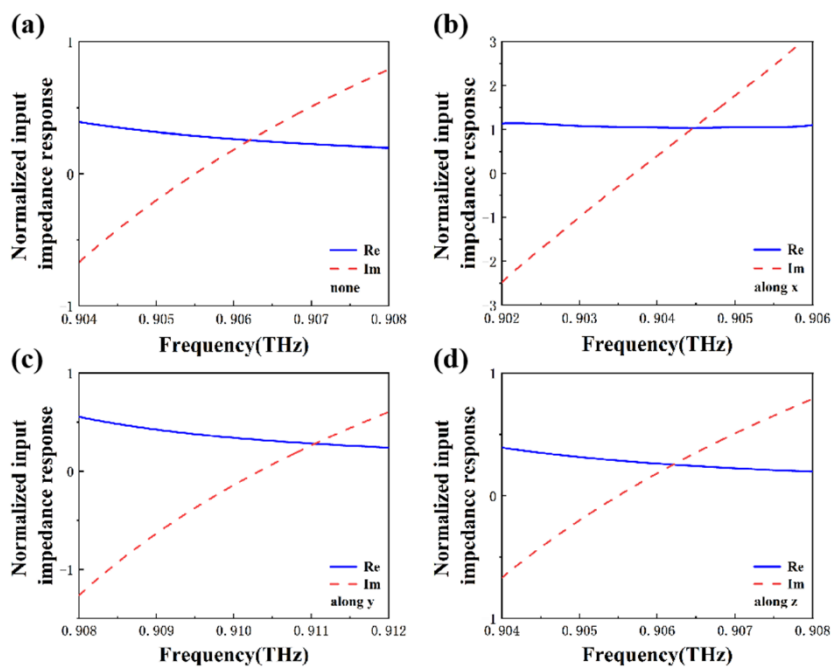


**Fig. 5** shows the normalized input impedance response in the first-order. (a) No applied magnetic field (b) applied magnetic field along x-axis (c) applied magnetic field along y-axis (d) applied magnetic field along z-axis

**Table 2** Absorption peak offset caused by first-order Mie resonance

| | Outfield situation | The frequency position of the absorption peak | Offset compared to no magnetic field |
|---|---|---|---|
| First order Mie resonance (0.88-0.94 THz) | no magnetic field | 0.907 THz | |
| | magnetic field along *x* | 0.904 THz | 0.003 THz redshift |
| | magnetic field along *y* | 0.910 THz | 0.003 THz blueshift |
| | magnetic field along *z* | 0.906 THz | 0.001 THz redshift |

Then we analyze and compare the absorption peaks and offsets caused by the first three Mie resonances of the proposed absorber according to the four external field environments. As depicted in Fig. 4 and Fig. 5, when the absorber has the first-order Mie resonance in the four external field environments, the absorption peaks correspond to the normalized input impedance responses. As depicted in Fig. 4 and Table 2, the absorption peaks caused by the first-order Mie resonance in the four external field environments are all higher than 0.75. The

comparison of absorption peaks in different external field environments and no magnetic field environments shows that the maximum offset is 0.003 THz, while the tunable performance is poor at this time.

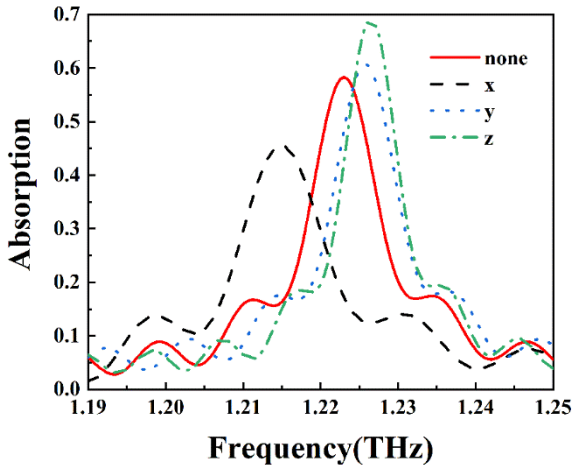


**Fig. 6** absorptivity caused by the second-order Mie resonance of the absorber under four external field environments

As depicted in Fig. 6 and Table 3, the maximum value of the absorption peak caused by the second-order Mie resonance in the four external field environments is 0.69. The comparison of absorption peaks in different external field environments and no magnetic field environments shows that the maximum offset is 0.008 THz, while the tunable performance is poor at this time.

**Table 3** Absorption peak offset caused by second-order Mie resonance

| | Outfield situation | The frequency position of the absorption peak | Offset compared to no magnetic field |
|---|---|---|---|
| Second order Mie resonance (1.19-1.25 THz) | no magnetic field | 1.223 THz | |
| | magnetic field along *x* | 1.215 THz | 0.008 THz redshift |
| | magnetic field along *y* | 1.226 THz | 0.003 THz blueshift |
| | magnetic field along *z* | 1.226 THz | 0.003 THz redshift |

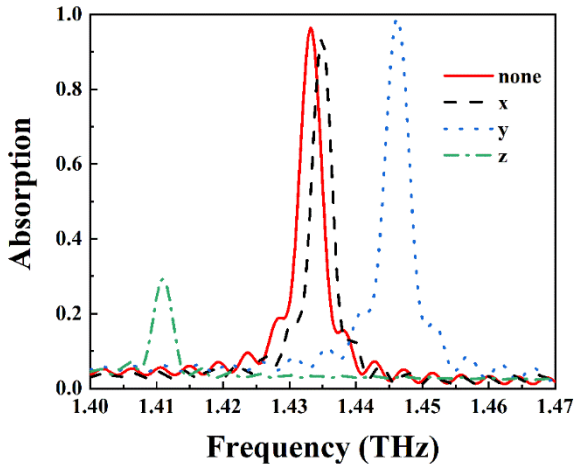


**Fig. 7** Absorptivity caused by the third-order Mie resonance of the absorber under four external field environments

As depicted in Fig. 7 and Table 4, the absorption peaks caused by the third-order Mie resonance in the four external field environments are 0.29 when the magnetic field is applied along the z direction, and the absorption peaks in the other three external field environments are all at 0.93 above. The comparison of absorption peaks in different external field environments and no magnetic field environments shows that the maximum offset is 0.022 THz, and the tunable performance is better at this time.

**Table. 4** Absorption peak offset caused by third-order Mie resonance

| | Outfield situation | The frequency position of the absorption peak | Offset compared to no magnetic field |
|---|---|---|---|
| Third order Mie resonance (1.40-1.47 THz) | no magnetic field | 1.433 THz | |
| | magnetic field along *x* | 1.435 THz | 0.002 THz redshift |
| | magnetic field along *y* | 1.446 THz | 0.013 THz blueshift |
| | magnetic field along *z* | 1.411 THz | 0.022 THz redshift |

The absorption peaks caused by the first three Mie resonances and the absorption peak offsets in no magnetic field environment and the magnetic field environment in three directions are analyzed and compared, and the result suggests that the first Mie resonance maintains a

large high absorption rate, whereas the offset of the absorption peak is significantly small, which is not a suitable research focus of this topic. The absorption rate of the second-order Mie resonance is less than 0.66 in different external field environments, and the offset of the absorption peak is very small, which is also not a suitable research focus of this topic. Except for the magnetic field along the z direction in the third-order Mie resonance, the absorption rate is higher than 0.93 in different external field environments, and the offset of the absorption peak is significant. The research focus will be placed on the third-order Mie resonance.

To achieve better tunability, the third-order Mie resonance peak is systematically analyzed. An absorber structure with efficient tunability in different external field environments is finally realized through continuous experiments and optimization adjustments. At the same time, proposed device also maintains high absorption performance within the simulation range.

**Table 5** Determines the final structural parameters through analysis and optimization

| Lattice constant (μm) | Microsphere radius (μm) | Spherical dielectric constant | Liquid crystal thickness (μm) | PI tape thickness (μm) | PI tape dielectric constant | Upper PI tape thickness (μm) | Upper PI tape dielectric constant |
|---|---|---|---|---|---|---|---|
| 118 | 30 | 33 | 165 | 6 | 3 | 15 | 3 |

We performed a parameter sweep during the design of this absorber and obtained a large number of simulation results. The scanned parameters include the lattice constant (100-140um), the radius of microspheres (25-35um), the dielectric constant of microspheres (28-36), the thickness of liquid crystal (100-200um), the thickness of PI tape (3-8um), the dielectric constant of PI tape (2.5-3.5), the thickness of upper PI tape (5-15um) and the dielectric constant of upper PI tape (2.5-3.5). The absorption peaks of the all-dielectric absorber in four external environments are analyzed. Finally, the structural parameters with large absorption peak offset and ideal absorption are determined. After continuous optimization, the final metasurface absorber structure parameters are as follows, as shown in Table 5.

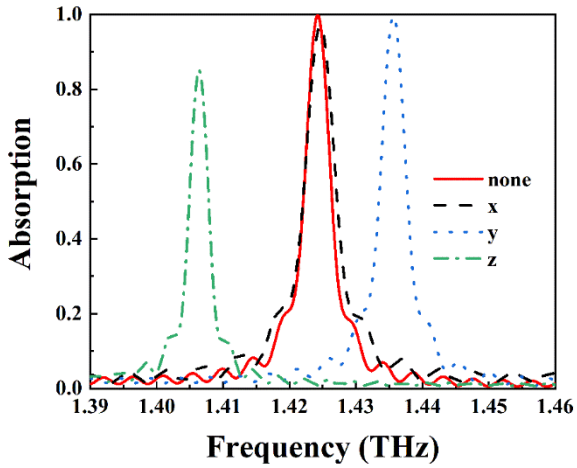


**Fig. 8** Absorption peaks caused by the third-order Mie resonance of the metasurface absorber determined in Table 5 under four external field environments

The absorption rate caused by the third-order Mie resonance is calculated according to the structure simulation of the absorber in Table 5, as shown in Fig. 8. When there is no magnetic field, the maximum absorption rate of 0.999 appears at 1.424 THz. When the applied magnetic field is along the x direction, the maximum value of the absorption rate of 0.968 appears at 1.425 THz, and a blueshift of 0.001 THz can be observed from 1.424 to 1.425 THz compared with no magnetic field. When the applied magnetic field is along the y direction, the maximum value of the absorption rate of 0.998 appears at 1.436 THz, and a blueshift of 0.012 THz can be identified compared with no magnetic field, from 1.424 to 1.436 THz. When the applied magnetic field is along the z direction, the maximum value of the absorption rate of 0.855 appears at 1.406 THz, compared with no magnetic field, a redshift of 0.018 THz can be observed, from 1.424 to 1.406 THz. For the third-order Mie magnetic resonance, a tunable maximum of 0.030 THz can be observed from 1.406 to 1.436 THz when the direction of the external magnetic field is changed from the *z* direction to the *y* direction. The result suggests that the absorption peaks of the structure in different external field environments are ideal, and the tunable range is relatively large. Under the three environments, including no external magnetic field, external magnetic field along the *x* direction, and external magnetic field along the y direction, the absorption rate has reached over 0.95; the absorption rate has reached over

0.85 and under the environment of the external magnetic field along the z direction. A tuning figure of merit (FOM) is introduced to quantify the resonance switching, which is given by [37]:

$$FOM = \frac{tuning\ range(THz)}{FWHM(THz)} \tag{10}$$

where FWHM is the full width at half the maximum resonance. The larger the FOM, the better the tunability. Here, the FOM of the magnetic resonance reaches 6.67, which shows that the all-dielectric absorber has good magnetic tunability.

**Table 6** Comparison of the performance of this work with other liquid crystal-based metasurface absorbers in the terahertz range

| References | Unit cell structure | Tuning method | The source of tuning | The tuning performance of the devices | Production process |
|---|---|---|---|---|---|
| [38] | NJU-LDn-4 NLC and silicon column array | electric field | internal | the absorption tuning range is only 0.01THz and the maximum absorption rate is close to 0.8 | medium |
| [39] | quartz glass and copper etched into a pattern | electric field | internal | the absorption tuning range is 0.01THz and the absorption rate is maintained above 0.9 | complicated |
| [40] | quartz glass and copper etched into a pattern | electric field | internal | the absorption tuning range is 0.02THz and the absorption rate is maintained above 0.9 | complicated |
| this work | zirconia microsphere and polyimide | magnetic field | external | the absorption tuning range is 0.03THz and the minimum absorption rate is higher than 0.85 | simple |

The experimental results suggest that the absorption peaks caused by the third-order Mie resonance of the structure are finally determined to be higher than 0.85, When the direction of the external magnetic field is changed from the z direction to the y direction, the maximum shift of the absorption peak is 0.030 THz, compared with the current research on liquid crystal tunable metamaterial absorbers [38-41], as shown in Table 6, the device proposed in this paper is simple to implement and has high efficiency tunable performance and absorption performance. In this work, the feasibility of effectively adjusting the absorption peak shift of all-dielectric metasurface absorbers proposed by theoretical analysis under different external magnetic field environments is verified by experiments.

## 4 Conclusion

In brief, there have been rare studies on tunable all-dielectric metasurface absorbers, whereas they have considerable application value in the terahertz range. By systematically studying the tunability performance of the respective absorption peak, we found that high-mode absorption peaks can achieve more efficient tunability. This study proposes a magnetically tunable all-dielectric metasurface absorber based on liquid crystals. Continuous experiments and optimization adjustments in different magnetic field scenarios have achieved a certain degree of shift in the absorption peak of the metasurface, and the absorption peak is more ideal. The all-dielectric metasurface absorber proposed in this study has the advantages of stable tunability, low loss, simple production process, low production cost, miniaturization, high compatibility, and easy transplantation to other devices, and so forth, and solves the problem of tunable absorber design in the terahertz range. The device proposed in this study has an extremely narrow bandwidth, which is conducive to the development and application of terahertz resonant switches and filters. It provides a general method for the design of tunable artificial metamaterial absorbers and opens up new prospects for artificial tunable devices in the terahertz band.

## Acknowledgments

The researchers would like to acknowledge Deanship of Scientific Research, Taif University for funding this work.

## Authors' Contributions

As per the journal requirement of more than ten contributors, the required contribution can be briefly stated as follows. Song Gao: conceptualization, methodology, validation, formal analysis, writing – original draft; Chuwen Lan: conceptualization, methodology, writing – review and editing; Xiaojun Zhai: conceptualization, resources, and writing – review and editing; Jianchun Xu, Jinqing Cao, Huiming Yao, S. Eltahir Ali, Hala M. Abo-Dief, Abdullah K. Alanazi, and Hassan Algadi: writing – review and editing.

## Funding

This work was supported by the National Natural Science Foundation of China (Nos. 62175016, 52102061).

## Conflict of Interest

The authors declare no conflict of interest.

## References

1. Li FS, Li QY et al (2023) Morphology controllable urchin-shaped bimetallic nickel-cobalt oxide/carbon composites with enhanced electromagnetic wave absorption performance. Journal of Materials Science & Technology 148:250-259. https://doi.org/10.1016/j.jmst.2022.12.003

2. Feng SX, Zhai FT et al (2023) Progress of metal organic frameworks-based composites in electromagnetic wave absorption. Materials Today Physics 30:100950. https://doi.org/10.1016/j.mtphys.2022.100950

3. Pan D, Yang G, Abo-Dief et al (2022) Vertically Aligned Silicon Carbide Nanowires/Boron Nitride Cellulose Aerogel Networks Enhanced Thermal Conductivity and Electromagnetic Absorbing of Epoxy Composites. Nano-Micro Letters 14:118. https://doi.org/10.1007/s40820-022-00863-z

4. Zhang Z, Li Z, Zhao Y et al (2022) Dielectric enhancement effect in biomorphic porous carbon-based iron@iron carbide 'meta-powder' for light-weight microwave absorption material design. Advanced Composites and Hybrid Materials 5:3176-3189. https://doi.org/10.1007/s42114-022-00445-y

5. Hu P, Dong S, Yuan F et al (2022) Hollow carbon microspheres modified with NiCo2S4 nanosheets as a high-performance microwave absorber. Advanced Composites and Hybrid Materials 5:469–480. https://doi.org/10.1007/s42114-021-00318-w

6. Du WY, Huang YY, Zhou YX, Xu XL (2022) Terahertz interface physics: from terahertz wave propagation to terahertz wave generation. Journal of Physics D-Applied Physics 55:223002. https://doi.org/10.1088/1361-6463/ac3f58

7. Mo B, Wang C (2022) Broadband and wideangle absorption of transparent conformal metamaterial. Advanced Composites and Hybrid Materials 5:383-389. https://doi.org/10.1007/s42114-021-00410-1

8. Sun K, Yang XC et al (2023) Core-shell structural design and microwave absorption enhancement of multi-dimensional graphene oxide@polypyrrole/carbonyl iron fiber nanocomposites. Journal of Alloys and Compounds 930:167446. https://doi.org/10.1016/j.jallcom.2022.167446

9. Yang PT, Sun K et al (2022) Negative Permittivity Behaviors Derived from Dielectric Resonance and Plasma Oscillation in Percolative Bismuth Ferrite/Silver Composites. The Journal of Physical Chemistry C 126:12889-12896. https://doi.org/10.1021/acs.jpcc.2c03543

10. Ferguson B, Zhang XC (2002) Materials for terahertz science and technology. Nature Materials 1:26-33. https://doi.org/10.1038/nmat708

11. Manikandan E, Princy SS, Sreeja BS, Radha S (2019) Structure Metallic Surface for Terahertz Plasmonics. Plasmonics 14:1311-1319. https://doi.org/10.1007/s11468-019-00974-1

12. Khurgin JB (2015) How to deal with the loss in plasmonics and metamaterials. Nature Nanotechnology 10:2-6. https://doi.org/10.1038/nnano.2014.310

13. West PR, Ishii S, Naik GV, Emani NK, Shalaev VM, Boltasseva A (2010) Searching for better plasmonic materials. Laser & Photonics Reviews 4:795-808. https://doi.org/10.1002/lpor.200900055

14. Khurgin JB, Sun G (2012) Practicality of compensating the loss in the plasmonic waveguides using semiconductor gain medium. Applied Physics Letters 100:11105. https://doi.org/10.1063/1.3673849

15. Liu WW, Li ZC, Cheng H, Chen SQ (2020) Dielectric Resonance-Based Optical Metasurfaces: From Fundamentals to Applications. Iscience 23:101868. https://doi.org/10.1016/j.isci.2020.101868

16. Headland D, Nirantar S, Withayachumnankul W, Gutruf P, Abbott D, Bhaskaran M, Fumeaux C, Sriram S (2015) Terahertz Magnetic Mirror Realized with Dielectric Resonator Antennas. Advanced Materials 27:7137-7144. https://doi.org/10.1002/adma.201503069

17. Fan KB, Suen JY, Liu XY, Padilla WJ (2017) All-dielectric metasurface absorbers for uncooled terahertz imaging. Optica 4:601-604. https://doi.org/10.1364/optica.4.000601

18. Belov V, Belov I, Harel L (1997) Preparation of spherical yttria-stabilized zirconia powders by reactive-spray atomization. Journal of the American Ceramic Society 80:982-990. https://doi.org/10.1111/j.1151-2916.1997.tb02930.x

19. Fang B, Feng DT et al (2021) All dielectric terahertz carpet cloaking by phase compensation metasurfaces. Laser Physics Letters 18:126201. https://doi.org/10.1088/1612-202X/ac3128

20. Wu F, Yu X, Panda A, Liu DJ (2022) Terahertz angle-independent photonic bandgap in a one-dimensional photonic crystal containing InSb-based hyperbolic metamaterials. Applied Optics 61:7677-7684. https://doi.org/10.1364/ao.470923

21. Leng J, Peng J et al (2022) Investigation of terahertz high Q-factor of all-dielectric metamaterials. Optics and Laser Technology 146:107570. https://doi.org/10.1016/j.optlastec.2021.107570

22. Xu J, Cao J et al (2021) Metamaterial mechanical antenna for very low frequency wireless communication. Advanced Composites and Hybrid Materials 4:761-767. https://doi.org/10.1007/s42114-021-00278-1

23. Wu Z, Zhang Z, Xu Y, Zhai Y, Zhang C, Wang B, Wang Q (2022) Random color filters based on an all-dielectric metasurface for compact hyperspectral imaging. Optics letters 47:4548-4551. https://doi.org/10.1364/ol.469097

24. Zhang C, Hu JP, Dong YG, Zeng AJ, Huang HJ, Wang CH (2021) High efficiency all-dielectric pixelated metasurface for near-infrared full-Stokes polarization detection. Photonics Research 9:583-589. https://doi.org/10.1364/prj.415342

25. Hou CX, Yang WY, Hideo Kimura et al (2023) Boosted lithium storage performance by local build-in electric field derived by oxygen vacancies in 3D holey N-doped carbon structure decorated with molybdenum dioxide. Journal of Materials Science & Technology 142:185-195. https://doi.org/10.1016/j.jmst.2022.10.007

26. Mu Q, Liu R, Kimura H et al (2023) Supramolecular self-assembly synthesis of hemoglobin-like amorphous CoP@N, P-doped carbon composites enable ultralong stable cycling under high-current density for lithium-ion battery anodes. Advanced Composites and Hybrid Materials 6:23. https://doi.org/10.1007/s42114-022-00607-y

27. Yang W, Peng D, Kimura H et al (2022) Honeycomb-like nitrogen-doped porous carbon decorated with Co3O4 nanoparticles for superior electrochemical performance pseudo-capacitive lithium storage and supercapacitors. Advanced Composites and Hybrid Materials 5:3146-3157. https://doi.org/10.1007/s42114-022-00556-6

28. Dang C, Mu Q, Xie X et al (2022) Recent progress in cathode catalyst for nonaqueous lithium oxygen batteries: a review. Advanced Composites and Hybrid Materials 5:606–626. https://doi.org/10.1007/s42114-022-00500-8

29. Ma Y, Xie X, Yang W et al (2021) Recent advances in transition metal oxides with different dimensions as electrodes for high-performance supercapacitors. Advanced Composites and Hybrid Materials 4:906-924. https://doi.org/10.1007/s42114-021-00358-2

30. Hou CX, Wang B, Vignesh Murugadoss et al (2020) Recent Advances in Co3O4 as Anode Materials for High-Performance Lithium-Ion Batteries. Engineered Science 11:19-30. https://dx.doi.org/10.30919/es8d1128

31. He XY, Lin FT, Liu F, Shi WZ (2020) Tunable strontium titanate terahertz all-dielectric metamaterials. Journal of Physics D-Applied Physics 53:155105. https://doi.org/10.1088/1361-6463/ab6ccc

32. Zeng XX, Wu LL, Xi XQ, Li B, Zhou J (2018) Thermally tunable terahertz magnetic responses of TbFeO3 ceramic. Ceramics International 44:19054-19057. https://doi.org/10.1016/j.ceramint.2018.07.088

33. Zhang FL, Kang L (2009) Magnetically tunable left handed metamaterials by liquid crystal orientation. Optics Express 17:4360-4366. https://doi.org/10.1364/OE.17.004360

34. Wheeler MS, Aitchison JS et al (2006) Coated nonmagnetic spheres with a negative index of refraction at infrared frequencies. Physical Review B 73:045105. https://link.aps.org/doi/10.1103/PhysRevB.73.045105

35. Lewin L (1947) The Electrical Constants of a Material Loaded with Spherical Particles. ProInst Electr Eng 94:65-68. https://10.1049/ji-3-2.1947.0013

36. Lepetit T, Akmansoy E et al (2011) Experimental evidence of resonant effective permittivity in a dielectric metamaterial. Journal of Applied Physics 109:77. https://doi.org/10.1063/1.3537920

37. Lan CW, Wu HL et al (2018) Magnetically tunable terahertz all-dielectric metamaterial based on liquid crystal. arXiv: Optics. https://doi.org/10.48550/arXiv.1808.01455

38. Zhou SH, Shen ZX et al (2018) Liquid Crystal Tunable Dielectric Metamaterial Absorber in the Terahertz Range. Applied Sciences 8:2211. https://doi.org/10.3390/app8112211

39. Deng GS, Hu HL et al (2022) Liquid crystal-based wide-angle metasurface absorber with large frequency tunability and low voltage. Optics Express 30:22550-22561. https://doi.org/10.1364/OE.462307

40. Deng GS, Hu HL et al (2021) Tunable terahertz metamaterial wideband absorber with liquid crystal. Optical Materials Express 11:4026-4035. https://doi.org/10.1364/OME.444899

41. David Shrekenhamer, Chen WC et al (2013) Liquid Crystal Tunable Metamaterial Absorber. Physical Review Letters 110:177403. https://doi.org/10.1103/PhysRevLett.110.177403

The graphical abstract:

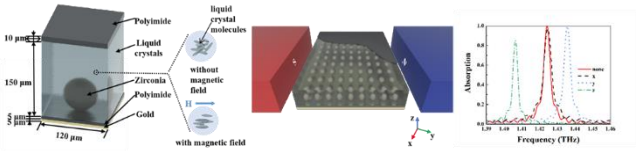


In the terahertz range, this work proposes to composite the all-dielectric metasurface and liquid crystal, and it is found that under the high mode of Mie resonance, the dielectric properties of the liquid crystal change due to the applied magnetic field, so as to realize the efficient active tuning of the absorber absorption peak.